Published in final edited form as:
Nanomedicine (Lond). 2014 January ; 9(1): 121–134. doi:10.2217/nnm.13.191.

Shaping cancer nanomedicine: The effect of particle shape on the *in vivo* journey of nanoparticles

Randall Toy[1,2,3], **Pubudu M. Peiris**[1,2,3], **Ketan B. Ghaghada**[4,5], and **Efstathios Karathanasis**[1,2,3,6,*]

[1]Department of Biomedical Engineering, Case Western Reserve University, Cleveland, OH 44106, United States

[2]Department of Radiology, Case Western Reserve University, Cleveland, OH 44106, United States

[3]Case Center for Imaging Research, Case Western Reserve University, Cleveland, OH 44106, United States

[4]Edward B. Singleton Department of Pediatric Radiology, Texas Children's Hospital, Houston, TX 77030, United States

[5]Department of Radiology, Baylor College of Medicine, Houston, TX 77030, United States

[6]Case Comprehensive Cancer Center, Cleveland, OH 44106, United States

Summary

Recent advances in nanoparticle technology have enabled the fabrication of nanoparticle classes with unique size, shape, and materials, which in turn has facilitated major advancements in the field of nanomedicine. More specifically, in the last decade, nanoscientists have recognized that nanomedicine exhibits a highly engineerable nature that makes it a mainstream scientific discipline, which is governed by its own distinctive principles in terms of interactions with cells and intravascular, transvascular and interstitial transport. This review focuses on recent developments and understanding of the relation between the shape of a nanoparticle and its navigation through different biological processes. Importantly, we seek to illustrate that the shape of a nanoparticle can govern its *in vivo* journey and destination dictating its biodistribution, intravascular and transvascular transport, and ultimately targeting of difficult-to-reach cancer sites.

Keywords

cancer; nanomedicine; nanoparticle shape; phagocytosis; biodistribution; margination; transport of nanoparticles; targeting avidity

[*]Author to whom correspondence should be addressed: Efstathios Karathanasis, Ph.D., 2071 Martin Luther King Jr. Drive, Wickenden Building, Cleveland, Ohio 44106, United States of America, Phone: 216.844.5281; Fax: 216.844.4987; stathis@case.edu.

Introduction

Due to the unique material properties that appear at the nanoscale, nanomedicine provides many benefits and new opportunities to tackle the complexity of cancer. The first success story of nanomedicine was the clinical approval of liposomal doxorubicin for clinical use [1], which marked the launch of the entire field. This early success was based on a unique feature that appears at the nanoscale. While conventional small molecular agents are distributed within cancer and healthy tissues in a non-specific manner, nanoparticles exploit the leaky vasculature of solid tumors to enhance the intratumoral drug delivery due to the so-called “Enhanced Permeability and Retention” (EPR) effect, which results in improved drug safety profiles and reduced off-target delivery [1–5]. Furthermore, nanomedicine’s multifunctional abilities to seek, search, and destroy has been exploited to develop various therapeutic, imaging, and theranostic agents, which are under preclinical and clinical evaluation [6]. In addition to the control over the size of nanoparticles, the engineerable nature of nanoparticles has led to nanostructures with various shapes [7, 8] and new properties [9, 10]. In this 50 year lifetime, nanomedicine has grown from an “exotic” research area to a mainstream scientific field. In this context, nano-engineers and nano-scientists have started to recognize that nanomedicine is governed by its own distinctive principles in terms of intravascular, transvascular and interstitial transport [11, 12], which dictate rules of designing a nanoparticle for highly site-specific delivery facilitating significant therapeutic enhancements for difficult-to-treat cancers.

Do the physical characteristics of nanoparticles matter?

To answer this question, we first have to consider that nanoparticles *en route* to their target face numerous biobarriers created by the host immune system as well as the tumor abnormal physiology, which includes physically compromised vasculature, erratic blood flow, abnormal extracellular matrix, and high interstitial fluid pressure. To overcome the tumor’s abnormal biobarriers, the first design rules were derived with respect to the effect of nanoparticle size on tumor dosing and anticancer efficacy [13–16]. For example, the development of long-circulating liposomal nanocarriers was the product of 30 years of intensive research, since Bangham first discovered the liposome in the early 1960s [17, 18]. More specifically, in the ‘80s and ‘90s, a large number of studies focused on the effect of size, composition and polymer coating of liposomal doxorubicin on its blood circulation, intratumoral accumulation and anticancer activity [19–29]. It was concluded that the nanoparticle’s size is a critical factor that determines blood circulation, which in turn relates to the tumor accumulation, tumor retention, and drug release [25, 30, 31]. Liposomes ranging between 40–700 nm in size were evaluated; it was found that liposomes larger than 200 nm generally do not extravasate into tumors [25]. Furthermore, these studies concluded that a PEGylated unilamellar liposome with a diameter between 50–150 nm displayed the most prolonged circulation time (blood 2nd phase $t_{1/2}$~55 h) and, as a result, an increased accumulation in tumors and antitumor activity [22, 25]. However, this size range was a compromise between the loading efficiency of liposomes (increases with increasing size), clearance by the reticuloendothelial system (increases with increasing size) and the ability to extravasate (decreases with increasing size) [32, 33]. However, this compromise did not take under consideration the uniqueness of each tumor. A close examination of the published

literature indicates a significant deviation from the mean *in vivo* performance leading to significant overlap between nanoparticles of different sizes [24–26, 34]. Importantly, the dependence of *in vivo* behavior on nanoparticle size follows predictable patterns based not only on the individual features of each tumor but also different regions within the same tumor [35–37]. Indeed, it was recently shown that the intravascular and transvascular transport of nanoparticles in a tumor's region is strongly governed by the relationship of particle size to the microvascular network and hemodynamics of that tumor's region [38]. Given that tumors are heterogeneous in both hemodynamics and pathology [35, 39–44], a single "one-size-fits-all" nanoparticle design might not be the most effective approach. We suggest that the nanoparticle design depends on the exact location of interest (e.g. primary or metastatic tumor, tumor stage and aggressiveness, host organ, regional vascular characteristics and hemodynamics).

Does the shape of a nanoparticle matter?

The overall transport of a circulating nanoparticle is due to movement from applied convective forces and, to a much lesser degree, Brownian motion [14]. First, the transvascular transport (e.g. extravasation) of nanoparticles is partially governed by the rate of fluid flow and filtration along a capillary, which depends upon the hydrostatic pressure gradient (i.e. the difference between the vascular pressure and interstitial flow pressure (IFP)) [45]. The typical IFP of solid tumors is typically much higher than that of normal tissues due to the higher vessel leakiness and reduced lymphatic drainage. Thus, the typical decreased blood flows and increased interstitial flow pressures (IFP) in tumors dictate the degree of resistance to extravasation of nanoparticles. In this context, as the particle size increases, faster blood flow patterns are required to overcome high IFP in tumors [38]. In fact, a recent clinical study demonstrated that transient increase of blood pressure (and subsequently tumor blood flow) resulted in enhanced delivery of nanoscale drugs to tumors that otherwise have modest EPR [46]. A preclinical study [47] showed that hyperthermia-induced increase of tumor blood flow enabled the extravasation 400-nm liposomes into human ovarian carcinoma, which otherwise is impermeable to even 100-nm liposomes.

However, an even more important process than transvascular transport is the one that has to occur before. One of the pivotal steps dictating the transport of flowing nanoparticles is their margination (i.e. radial drift) towards the blood vessel walls. Near-the-wall margination is not just desirable. It is required for a nanoparticle to interact with the tumor vascular bed and have subsequent meaningful interactions. Obviously, this is critical not only when the site of interest is the tumor interstitium (e.g. cancer cell targeting), but also the tumor vasculature (e.g. vascular targeting). Since nanoparticles are primarily transported in the tumor microcirculation via convective means, margination is not favored. Contrary to spherical nanoparticles, oblate-shaped nanoparticles are subjected to torques resulting in tumbling and rotation, which increase the lateral drift of nanoparticles towards the blood vessel walls in microcirculation [13, 48, 49].

In addition to transport, the shape of nanoparticles has been shown to dictate the interaction of nanoparticles with cell membranes. First, the shape of nanoparticles has been xshown to dictate their clearance by macrophages of the reticuloendothelial organs. Recent studies

have indicated that the oblate shape of particles favors their circulation in the blood due to lower uptake by macrophages [50–53]. Subsequently, this prolongs the blood residence of nanoparticles and increases their chances of reaching their target site. Besides macrophages, the nanoparticle shape seems to also dictate endocytosis by normal and cancer cells. Furthermore, targeting nanoparticles using receptor-ligand systems is also governed by shape. To maximize the specificity towards sites of interest, cancer cell targeting or vascular targeting strongly depends on the targeting avidity of nanoparticles. Compared to nanospheres, oblong-shaped nanoparticles are able to form a greater number of multivalent occurrences [54]. This is essential for targeting especially in the case of vascular targets, since geometrically enhanced targeting can effectively offset hemodynamic forces that tend to detach the nanoparticle from the endothelium [55].

Importantly, understanding the design rules for improved margination and vascular targeting of nanoparticles can facilitate diagnosis and treatment of the most aggressive forms of cancer. While potent cytotoxic agents are available to oncologists, the clinical utility of these agents is limited by their toxicity to normal tissues, which leads to use of suboptimal doses for eradication of metastatic disease [56]. Additionally, the small size, high dispersion to organs, and low vascularization of micrometastases makes them nearly inaccessible to drugs. To date, applications of nanomedicine have mainly focused on primary tumors. While the EPR strategy may be effective in well-vascularized primary tumors larger than 100 mm^3, it is ineffective with micrometastatic disease, which presents small clusters of malignant cells within variable tissue types [57, 58]. Considering that the vast majority of cancer deaths are due to metastatic disease [59], the most effective strategy to reach micrometastases may be to design nanomedicines capable of highly selective delivery to micrometastases *via* vascular targeting of biomarkers on the endothelium associated with metastatic disease. Thus, “shaping” nanomedicine can provide new opportunities to address important and unmet clinical needs.

How much control can we have over the shape of nanoparticles?

Numerous fabrication methods have enabled the creation of non-spherical nanoparticles with a wide range of different sizes and shapes with high precision (Table 1). These nanoparticles are manufactured from a wide range of materials and also vary in flexibility. Using different methods, particles are generated with two-dimensional polygonal shapes [60–67], three-dimensional polyhedral shapes [68–72], rod shapes [73–79], branched structures [80–83], and other complex shapes such as snowflakes [81], flowers [81], thorns [81], hemispheres [84, 85], cones [85, 86], urchins [87, 88], filamentous particles [52], biconcave discoids [89], worms [8], trees [90], dendrites [91], necklaces [92], and chains [9, 55, 93, 94]. Importantly, the ability to produce drug product with a high level of consistency and reproducibility is critical in the pharmaceutical industry. Needless to say, the field of nanotechnology presents its own challenge, since it is a highly diverse new area. However, various nanomanufacturing methods (e.g. liposomal drugs, iron oxide nanoparticles) have already demonstrated reproducibility and scalability, which enabled the manufacturing process to be transferred to a Good Manufacturing Practice (GMP) facility for production of GLP- and GMP-grade material. In this context of translation of nanomedicine from bench to bedside, besides the obvious importance in clinical trials, scalable and consistent

nanomanufacturing accelerates preclinical tests including Investigation of New Drug (IND)-enabling safety and toxicity studies as well as efficacy in large animal models. Along those lines, adjusting existing methods can fabricate both spherical and non-spherical nanoparticles with similar ease. For example, the gold nanoparticle synthesis method employing deep eutectic solvents (DES) produces a wide variety of different particle shapes through small adjustments in stoichiometry [81]. Another top-down fabrication method, Particle Replication in Non-wetting Templates (known as PRINT), uses lithography to produce nanoparticles of all shapes with the same ease [95]. Furthermore, a nanofabrication technology based on Dip-Pen nanolithography has enabled commercial manufacturing of nanoparticles of various shapes and structures from a variety of different materials [96]. In addition, by adapting a solid-phase chemistry strategy, nanospheres can be assembled into oblong chain-like nanoparticles of various aspect ratios, which can be scaled up relatively easily [9].

While nanoparticle size and surface characteristics have been reviewed elsewhere [97], this review focuses exclusively on the importance of shape as an essential property of nanoparticles that plays an ultimate role in various biological processes [95, 98, 99]. In the proceeding sections, we will illustrate how a nanoparticle's shape influences its biodistribution, ability to marginate and escape the blood flow, and binding affinity to the receptors it targets (Figure 1).

The effect of nanoparticle shape on biodistribution and macrophage uptake

For a nanoparticle to successfully travel to and bind to its biological target, it must first be able to travel in the bloodstream while evading uptake by macrophages, particularly in the reticuloendothelial system. Nanoparticle size was first identified as a critical parameter which affects the rate of macrophage uptake [102, 103]. Particles less than 5 nm are rapidly cleared from the circulation through extravasation or renal clearance [104, 105], and as particle size increases from the nanometer range to ~15 μm, accumulation occurs primarily in the liver and the spleen [106, 107]. In addition, studies have shown that PEG-coated spherical nanoparticles with neutral charge exhibit increased blood residence times [108]. While these studies with spherical particles have resulted in valuable insights, nanoparticle shape has also been established as an important parameter that dictates the rate of macrophage uptake [53]. In a study comparing the uptake of six distinct classes of nanoparticles with different shapes, a contact angle parameter was formulated, which was quantitatively related to particle internalization velocity. If a particle with a very high aspect ratio (~20) aligns with its long axis parallel to the cell membrane, it will internalize more slowly than a particle which aligns with its short axis parallel to the cell membrane (Figure 2). In support of these findings, computational simulations evaluating particle engulfment demonstrated that spheroidal particles internalized 60% more quickly when they were engulfed with their tips first [109]. Interestingly, nanoparticles that have a high rate of attachment may sometimes have a slow internalization rate [51]. An experiment which decoupled the attachment and internalization rates of nanoparticles found that prolate ellipsoids (major axis 0.35 – 2 μm, minor axis 0.2 – 2 μm) had both the highest attachment rate and slowest internalization rate in comparison to spheroidal (radius 0.26 – 1.8 μm) and oblate ellipsoidal nanoparticles (major axis 0.35–2.5 μm, minor axis 0.2–2 μm).

Biodistribution studies have also demonstrated that the uptake of spherical particles is favored over the uptake of particles with high aspect ratios in macrophages. For example, the liver uptake of 100-nm-long nanochains with an aspect ratio of about 4 was significantly lower than that of nanospheres with a 100-nm diameter [93]. Taking under consideration that nanoparticles are primarily cleared by the reticuloendothelial system, the low uptake of nanochains by the liver correlated to prolonged blood residence. Subsequently, the nanochains outperformed the 100-nm nanospheres in terms of extravasation into tumors, since nanoparticle extravasation into tumors is directly proportional to their blood residence time [110]. Another study evaluated the blood circulation of filomicelles, which are elongated assemblies of polymer micelles that have the ability to change in size *in vivo* over time [52]. Shear forces from blood flow act on portions of the filomicelle not in contact with the cell; these forces pull the nano-carrier away from the cell before it can be internalized. In the liver and spleen, the uptake of gold nanorods (size = 10 × 45 nm, AR = 4.5) was shown to be less than the uptake of gold nanospheres [111]. A biodistribution study with mesoporous silicon nanoparticles with an aspect ratio of 5 (length of 720 nm) had 50% of the liver uptake rate of particles with an aspect ratio of 1.5 (length of 185 nm) [112]. In the spleen, however, the uptake after 2 hours was nearly 3 times higher for nanorods with the aspect ratio of 1.5. Thus, it can be concluded that both nanoparticle size and aspect ratio play a role in organ-specific uptake. In addition, the rate of phagocytosis for a nanoparticle of a particular geometry may be organ-dependent.

Modifying nanoparticle shape to enhance margination

After a nanoparticle successfully evades phagocytosis via macrophages and reaches its target site, it must be able to escape the blood flow and marginate towards the wall of the blood vessel. Nanoparticle margination is dictated by forces which influence particle translational and rotational motion, which include buoyancy, gravity, drag, van der Waals interactions, electrostatic double layer interactions, and steric repulsive interactions. Under a balance of these forces, spherical nanoparticles tend to follow the streamlines of the flow they are traveling in [113, 114]. The tendency for a spherical nanoparticle to marginate is dependent on its size [115, 116]. The transport of large spherical nanoparticles is heavily driven by convection, which results in a higher difficulty to escape the flow and move towards the vessel wall. On the contrary, the transport of smaller nanoparticles exhibits a relatively higher diffusion component, which allows them to move laterally in the blood vessel with greater ease. This was demonstrated in a study which found that a 65 nm liposome had a 3.4 times higher margination rate than a 130 nm liposome [116].

Unlike spherical nanoparticles, rod-shaped nanoparticles experience lateral drift that varies depending on the angle of their orientation (Figure 3) [113, 117]. The tendency for rods to drift may be explained by the variable drag forces and torques that are exerted on rods under flow, which influence their ability to marginate. In fact, discoidal (AR = 0.5), hemisphere, and ellipsoidal particles (AR = 0.5) also have higher drift velocities than spheres [13]. For different classes of discoidal particles, the drift velocity increases as the particle aspect ratio deviates further away from one. Of the ellipsoids, hemispheres, and discs, it was found that discoidal particles most prominently follow highly oscillatory trajectories that lead to increased interactions with the vessel wall.

In light of these findings, researchers have developed *in vitro* methods to study the effect of nanoparticle shape on margination [13, 49, 116, 118–120]. Primarily, studies have compared the margination of four classes of particles: spheres, rods, ellipsoidal particles, and discoidal particles. These studies are typically conducted in parallel plate flow chambers and microfluidic flow chambers, which allow experimentation to be conducted at controlled flow rates [115, 116]. One recent study compared the margination of nanoparticles below 200 nm in diameter in rectangular microfluidic flow networks [116]. It was observed that when shear rate was decreased, the margination of nano-spheres increased almost two-fold. Shape also played a major role in enhancing nanoparticle margination; nano-rods (56 nm × 25 nm; AR ~ 2) had 7-fold higher accumulation than nano-spheres under the same shear rate. Similar results were observed when the margination rate of an oblong iron oxide nanochain (100 × 20 nm; AR=5) was compared to a 20-nm iron oxide nanosphere in a microfluidic flow network setup [55]. At a flow rate of 50 μL/min, which is in the range of expected blood flow in tumor microcirculation, the nanochain exhibited 2.3-fold higher margination than the IO sphere. Differences in blood hematocrit also have an effect on nanoparticle margination [119, 121]. Another study evaluated the effect of shape and flow rate simultaneously using mesoporous spherical, rod-like, and disc-like particles [118]. When particle width was held constant, discs marginated two times more than rods. Differences in adhesion are likely to be the dominant cause for lower particle adhesion, as high shear rates easily dislodge adhered particles. Yet, we also postulate that high shear rates hinder particle margination because it is more difficult for nanoparticles to escape fast flows. Vessel geometry is also a critical consideration for the evaluation of nanoparticle margination; in general, particles deposit at higher levels at a vessel bifurcation than along a straight vessel [120]. Shape, however, can further enhance the increase in deposition at the vessel junction – flowing ellipsoidal discs displayed a 2–2.5 fold higher ratio of bifurcation to straight vessel wall attachment than spheres. Thus, the advantages of oblate shapes may be even greater in the complex vessel geometries commonly found *in vivo*.

Recent studies have also focused on improving the *in vitro* experimental design to more accurately represent physiological conditions. As laminar and shear flows are highly idealized, nanoparticle margination has also been recently evaluated under pulsatile flows and recirculating flows [119]. Both particle size and aspect ratio were again identified as key determinants that affect the level of margination. For 1 and 2 μm particles in pulsatile flow, high aspect ratio rod-shaped particles ($9 < AR < 11$) had 2 times higher binding than spherical particles. A similar enhancement in binding was observed when the same classes of particles were subjected to recirculating flow. The trajectory of nanoparticles *in vivo* is also impacted by particle interactions with circulating red blood cells (RBC) and leukocytes. Red blood cells have a tendency to remain in the middle of the blood flow, which creates a “cell free” layer that depends on the blood flow rate. In contrary, the oblong shape of leukocytes allows them to escape the blood flow, which allows them to move within the RBC-free layer [122]. Nanoparticles in circulation collide with both red blood cells and leukocytes, which influence their margination behavior. Experimentally, it has been found that increasing hematocrit from 30% to 45% enhances the margination and binding of 2 μm particles 2-fold [121]. At higher hematocrits, the ratio of rod to sphere margination and binding is also increased [119].

Tailoring nanoparticle shape to maximize binding avidity

After marginating to the wall of a blood vessel, a nanoparticle must be able to bind to its target of interest, which is usually a cluster of receptors that are over-expressed on the cell surface. Unlike small molecule targeting agents that display a single ligand, nanoparticles are able to exhibit multiple ligands on their surface, which results in an avidity-based targeting [123]. As a result, several low binding ligands can work in tandem to create a high-affinity nanoparticulate construct for targeting multiple receptors over-expressed on target cells [124]. Thus, while the ligand-bearing nanoparticles have high affinity, several other factors are known to influence their binding to cell-surface receptors. For example, increasing the nanoparticle's size (i.e. decreasing its curvature), while keeping the surface ligand density constant, will increase the number of bonds between the nanoparticle and the cell. Another effective way to enhance binding avidity is to alter the nanoparticle shape, which changes the way in which ligands are presented on the particle surface (Figure 4). Nanoparticles of different shapes have a different active fractional area (AFAC), which results in variability in binding avidity. It is important to note that the flexibility and density of the ligands on the particle surface also affects binding avidity [125–128]. The use of flexible polymeric chains, such as polyethylene glycol (PEG), for presenting ligands result in a larger volume for interaction with cell surface receptors and therefore a high probability for the formation of receptor-ligand bonds [129]. The length of the polymer has also been shown to influence binding of nanoparticles [126, 130, 131]. For a 100 nm particle, tripling the molecular weight of the PEG used will also triple the AFAC. In certain cases, where the presence of ligands is known to reduce the blood half-life of nanoparticles, the nanoparticles are decorated with an additional layer of 'stealth' polymer. In such cases, an understanding of the interplay between the two different types of polymer chain length and their surface density becomes important to ensure sufficient binding efficiency to target receptors while maintaining the desired blood half-life of the targeted nanoparticles [132].

Both *in vitro* and *in vivo* studies have demonstrated the influence of particle shape and size on the binding efficiency of nanoparticles [88, 133]. A recent study has shown that anti-iCAM spheres are internalized more quickly by endothelial cells than anti-iCAM discs of comparable size [88]. These spheres also were processed into lysosomal compartments and degraded more quickly than their discoidal counterparts. Rods targeted to ovalbumin, on the other hand, have twice as many specific binding interactions as ovalbumin-targeted spheres [133]. Binding avidity has also proven to be critical for vascular targeting. Successful vascular targeting requires that a nanoparticle can escape the blood flow and drift towards the blood vessel walls, followed by strong attachment to the targeting site offsetting the blood flow forces that tend to detach the particle. The targeting avidity of an $\alpha_v\beta_3$ integrin-targeting oblate shaped nanochain was assessed under flow in a microfluidic device coated with TNF-α-treated BAEC cells [55]. At only 5 min, the nanochain achieved 9.5-fold higher attachment compared to their $\alpha_v\beta_3$ integrin-targeting spherical counterparts (20 nm in diameter).

For the successful maximization of binding affinity through the adjustment of particle shape, ligand density, and ligand flexibility, the dynamics of the targeted receptor must also be considered. Receptors are often distributed and organized in a clustered, heterogeneous

pattern or a semi-homogenous pattern involving a combination of individually and clustered distribution. The folate receptor, a GPI-anchored receptor over-expressed in a variety of solid tumors, is distributed within small nano-sized lipid raft clusters [134, 135]. Transferrin receptor, a trans-membrane receptor over-expressed in brain tumors, is known to be clustered in coated pits as well as diffusively distributed on the cell surface [136]. Furthermore, some of the receptors, such as epidermal growth factor receptor (EGFR), are known to alter their surface distribution and enter into a clustered distribution upon ligand binding [137]. Since the binding event is often followed by receptor-mediated endocytosis, identifying the receptor internalization pathway is also important for understanding the route for intracellular entry of targeted nanoparticles [138–140]. The receptor-mediated internalization pathways can broadly be divided into: (1) clathrin-coated pits (CCP) pathway (2) caveolae-mediated pathway, and (3) lipid rafts pathway. A number of transmembrane proteins such as transferrin receptor, EGFR and low density lipo-protein (LDL) receptor are endocytosed via the CCP pathway. The folate receptor is internalized via the lipid rafts (also known as microdomains) pathway. In certain cases, the degree of internalization also depends on the cellular content of the exogenous ligand. For instance, the internalization dynamics of the folate receptor are governed by the cellular folate content [141]. An increase of intracellular folate content from 0.5 pmol to 1 pmol per million cells will result in a 75% decrease in folate binding affinity. Finally, the steric hindrance effects and access of receptor sites that arise due to the size and shape of nanoparticles should also be taken into consideration when evaluating binding and internalization [142].

Overall, we should carefully consider that binding of targeted nanoparticles to surface receptors is maximized at an optimal number of ligands per nanoparticle [143]. Surface presentation of very few ligands cannot achieve sufficient binding avidity, whereas too many ligands create steric hindrance and consume more receptors than necessary decreasing the binding chances of the nanoparticles [54]. At the same time, it is also necessary to consider the force necessary to translocate targeted nanoparticles of different shapes from the cell surface [144]. Increasing the maximum contact area of the nanoparticle by doubling its radius will lead to a 3-fold increase in the necessary force for particle translocation. Thus, an optimal combination of nanoparticle shape and ligand density has to be considered to facilitate targeting based on geometrically-enhanced multivalent docking and subsequent nanoparticle endocytosis.

Effect of nanoparticle shape on tumor deposition and therapeutic efficacy

Given that the shape of a nanoparticle affects its blood circulation, ability to marginate, and binding affinity, it is expected that a nanoparticle’s shape will also affect its rate of tumor deposition and therapeutic efficacy. Nanoparticle size has been extensively shown to affect the rate of nanoparticle intratumoral deposition through the EPR effect and subsequent therapeutic efficacy [19, 24]. These studies identified 100 nm as the optimal diameter for the deposition of spherical nanoparticles into tumors, which is dependent on vascular pore size, pharmacokinetics, and the ability to overcome high interstitial pressures through flow driven convection. In addition to different tumor microvascular systems (e.g. size of gaps on the endothelium, interstitial pressures, microvessel density, vasculature geometry), different tumor types have distinct vascular wall pore shapes. Therefore, the nanoparticle’s aspect

ratio may also determine unique extravasation rates and patterns into different tumors [145]. In an LS174T tumor, quantum dots extravasated four times more than carbon nanotubes with equivalent surface area; in an U87MG tumor, however, only the carbon nanotubes could extravasate. Higher aspect ratio also increased the delivery of nanoparticles to overexpressed vascular targets in a tumor. The ability of nanochains to perform vascular targeting was evaluated *in vivo* in the orthotopic 4T1 mammary adenocarcinoma model in mice [55]. At t=45 min after injection, vascular targeting of the nanochains resulted in a 2-fold higher tumor targeting than their spherical variant. At that time point, vascular targeting resulted in more than 40% of the administered nanochains being localized in the primary tumor.

The tailoring of nanoparticle shape also has improved the efficacy of tumor therapy. In particular, the use of an oblate shape increases the targeted delivery of antibody-displaying nanoparticles [146]. For example, trastuzumab coated nanorods exhibited a 5-fold greater cellular growth inhibition of when BT-474 breast cancer cells compared to equivalent nanospheres at the same nanoparticle dose [146]. This can be likely attributed to the 66% increase in binding and uptake by the cells of the nanorods compared to the nanospheres.

Besides cell culture studies, similar findings have been seen in tumors *in vivo.* Recently, it was shown that an 100-nm-long oblong chain-like nanoparticle (termed nanochain) composed of three iron oxide nanospheres and one doxorubicin-loaded liposome exhibited a 2-fold higher extravasation into tumors in a mammary adenocarcinoma model compared to spherical liposomal doxorubicin [93]. In addition, as a result of the multicomponent design of the nanochain, radiofrequency-triggered drug release from the particles resulted in the therapeutic efficacy being three-fold higher than treatments using spherical nanoparticles [93, 147]. Interestingly, the chain-shaped nanoparticle responded in a unique manner in the presence of a magnetic field. When magnetic nanoparticles are subjected to an external, oscillating magnetic field, there are two relaxation mechanisms (Brownian and Néel relaxation) that govern their magnetization response in an effort to align with the applied field. Brownian relaxation, the physical rotation of the entire nanoparticle, is typically the dominant relaxation mechanism for nanoparticles larger than about 25 nm. In the case of nanochains, Brownian relaxation is restricted by the bonds between the constituent nanospheres, such that Brownian motion may be observed as a mechanical “vibration” of the chain, rather than true rotational motion. Néel relaxation (reorientation of the particle’s magnetic moment with the applied field) is dominant for nanoparticles smaller than 15 nm. The size of the constituent iron oxide nanospheres in the nanochains places them in between the Brownian and Néel regimes, resulting in mechanical vibration that causes rapid and significant drug release. Therefore, beyond the shape and the size, composition, surface charge and polymer coating of nanoparticles, non-spherical nanoparticles result in new unique properties. The use of non-spherical gold nanoparticles over spherical gold nanoparticles is also advantageous in the application of photothermal triggered therapy. When nanorods were used in place of nanospheres, the photothermal absorption efficiency of the particle increased by 10-fold, which resulted in improved therapeutic efficacy [148].

Future perspective

Shape plays an instrumental role in determining the *in vivo* fate of a nanoparticle. This review highlighted studies assessing how shape affected a nanoparticle's ability to evade immune uptake, escape the blood flow to travel to its target, and bind to its target with high affinity. Although spherical nanoparticles have been traditionally employed for tumor targeting due to their relative ease of fabrication, many recent findings suggest that non-spherical nanoparticles (e.g. rods, discs, hemispheres, ellipsoids) may target tumors more effectively. To make definitive conclusions on the best choice for nanoparticle shape, more comprehensive studies encompassing reticuloendothelial system clearance, margination, and cell attachment must be conducted. For a single set of nanoparticles with well-defined geometries, we must quantitatively determine and compare nanoparticle biodistribution, margination, and binding avidity. Subsequently, this quantitative information should be correlated to the therapeutic efficacy of nanoparticles of different shapes. It is important that we conduct these studies with ligands and receptors of oncologic relevance and in systems that accurately model *in vivo* geometry, morphology, and rheology. By considering nanoparticle shape alongside nanoparticle size and material, nanoparticles may be engineered in a manner which will allow them to enter and treat tumors more effectively.

Acknowledgments

Financial Disclosure/Acknowledgements: This work was supported by grants from the National Cancer Institute (1R01CA177716), the Clinical and Translational Science Collaborative of Cleveland (UL1TR000439) from the National Center for Advancing Translational Sciences component of the National Institutes of Health, and the Ohio Cancer Research Associates (EK). R.T. was supported by a fellowship from the NIH Interdisciplinary Biomedical Imaging Training Program (5T32EB007509).

References

1. Lasic DD, Papahadjopoulos D. Liposomes revisited. Science. 1995; 267(5202):1275–1276. [PubMed: 7871422]
2. Maeda H, Wu J, Sawa T, Matsumura Y, Hori K. Tumor vascular permeability and the EPR effect in macromolecular therapeutics: a review. J Control Release. 2000; 65(1–2):271–284. [PubMed: 10699287]
3. Gradishar WJ, Tjulandin S, Davidson N, et al. Phase III trial of nanoparticle albumin-bound paclitaxel compared with polyethylated castor oil-based paclitaxel in women with breast cancer. J Clin Oncol. 2005; 23(31):7794–7803. [PubMed: 16172456]
4. Lasic DD. Doxorubicin in sterically stabilized liposomes. Nature. 1996; 380(6574):561–562. [PubMed: 8606781]
5. Safra T. Cardiac safety of liposomal anthracyclines. Oncologist. 2003; 8 (Suppl 2):17–24. [PubMed: 13679592]
6. Ferrari M. Cancer nanotechnology: opportunities and challenges. Nat Rev Cancer. 2005; 5(3):161–171. [PubMed: 15738981]
7. Park JH, Von Maltzahn G, Zhang L, et al. Systematic surface engineering of magnetic nanoworms for in vivo tumor targeting. Small. 2009; 5(6):694–700. [PubMed: 19263431]
8. Park JH, Von Maltzahn G, Zhang LL, et al. Magnetic iron oxide nanoworms for tumor targeting and imaging. Advanced Materials. 2008; 20(9):1630–1635. [PubMed: 21687830]
9. Peiris PM, Schmidt E, Calabrese M, Karathanasis E. Assembly of linear nano-chains from iron oxide nanospheres with asymmetric surface chemistry. PLoS One. 2011; 6(1):e15927. [PubMed: 21253600]

10. Decuzzi P, Pasqualini R, Arap W, Ferrari M. Intravascular delivery of particulate systems: does geometry really matter? Pharm Res. 2009; 26(1):235–243. [PubMed: 18712584]
11. Jain RK. Delivery of molecular and cellular medicine to solid tumors. Adv Drug Deliv Rev. 2001; 46(1–3):149–168. [PubMed: 11259838]
12. Yuan F. Transvascular drug delivery in solid tumors. Semin Radiat Oncol. 1998; 8(3):164–175. [PubMed: 9634493]
13*. Lee SY, Ferrari M, Decuzzi P. Shaping nano-/micro-particles for enhanced vascular interaction in laminar flows. Nanotechnology. 2009; 20:495101, 11. Modeled the trajectories of spheroidal, ellipsoidal, discoidal, and hemisphere nanoparticles under different flow conditions. [PubMed: 19904027]
14. Decuzzi P, Causa F, Ferrari M, Netti PA. The effective dispersion of nanovectors within the tumor microvasculature. Ann Biomed Eng. 2006; 34(4):633–641. [PubMed: 16568349]
15. Decuzzi P, Ferrari M. Design maps for nanoparticles targeting the diseased microvasculature. Biomaterials. 2008; 29(3):377–384. [PubMed: 17936897]
16. Gentile F, Ferrari M, Decuzzi P. The transport of nanoparticles in blood vessels: the effect of vessel permeability and blood rheology. Ann Biomed Eng. 2008; 36(2):254–261. [PubMed: 18172768]
17. Papahadjopoulos D, Bangham AD. Biophysical properties of phospholipids. II. Permeability of phosphatidylserine liquid crystals to univalent ions. Biochim Biophys Acta. 1966; 126(1):185–188. [PubMed: 5970540]
18. Bangham AD, Papahadjopoulos D. Biophysical properties of phospholipids. I. Interaction of phosphatidylserine monolayers with metal ions. Biochim Biophys Acta. 1966; 126(1):181–184. [PubMed: 5970539]
19. Mayer LD, Tai LC, Ko DS, et al. Influence of vesicle size, lipid composition, and drug-to-lipid ratio on the biological activity of liposomal doxorubicin in mice. Cancer Res. 1989; 49(21):5922–5930. [PubMed: 2790807]
20. Gabizon A, Papahadjopoulos D. Liposome formulations with prolonged circulation time in blood and enhanced uptake by tumors. Proc Natl Acad Sci U S A. 1988; 85(18):6949–6953. [PubMed: 3413128]
21. Lasic DD, Martin FJ, Gabizon A, Huang SK, Papahadjopoulos D. Sterically stabilized liposomes: a hypothesis on the molecular origin of the extended circulation times. Biochim Biophys Acta. 1991; 1070(1):187–192. [PubMed: 1751525]
22. Papahadjopoulos D, Allen TM, Gabizon A, et al. Sterically stabilized liposomes: improvements in pharmacokinetics and antitumor therapeutic efficacy. Proc Natl Acad Sci U S A. 1991; 88(24): 11460–11464. [PubMed: 1763060]
23. Klibanov AL, Maruyama K, Torchilin VP, Huang L. Amphipathic polyethyleneglycols effectively prolong the circulation time of liposomes. FEBS Lett. 1990; 268(1):235–237. [PubMed: 2384160]
24. Nagayasu A, Shimooka T, Kinouchi Y, Uchiyama K, Takeichi Y, Kiwada H. Effects of fluidity and vesicle size on antitumor activity and myelosuppressive activity of liposomes loaded with daunorubicin. Biol Pharm Bull. 1994; 17(7):935–939. [PubMed: 8000381]
25. Nagayasu A, Uchiyama K, Kiwada H. The size of liposomes: a factor which affects their targeting efficiency to tumors and therapeutic activity of liposomal antitumor drugs. Adv Drug Deliv Rev. 1999; 40(1–2):75–87. [PubMed: 10837781]
26. Nagayasu A, Uchiyama K, Nishida T, Yamagiwa Y, Kawai Y, Kiwada H. Is control of distribution of liposomes between tumors and bone marrow possible? Biochim Biophys Acta. 1996; 1278(1): 29–34. [PubMed: 8611603]
27. Charrois GJ, Allen TM. Rate of biodistribution of STEALTH liposomes to tumor and skin: influence of liposome diameter and implications for toxicity and therapeutic activity. Biochim Biophys Acta. 2003; 1609(1):102–108. [PubMed: 12507764]
28. Awasthi VD, Garcia D, Goins BA, Phillips WT. Circulation and biodistribution profiles of long-circulating PEG-liposomes of various sizes in rabbits. Int J Pharm. 2003; 253(1–2):121–132. [PubMed: 12593943]

29. Ishida O, Maruyama K, Sasaki K, Iwatsuru M. Size-dependent extravasation and interstitial localization of polyethyleneglycol liposomes in solid tumor-bearing mice. Int J Pharm. 1999; 190(1):49–56. [PubMed: 10528096]
30. Bolotin E, Cohen R, Bar L, et al. Ammonium sulfate gradients for efficient and stable remote loading of amphipathic weak bases into liposomes and ligandoliposomes. Journal of Liposome Research. 1994; 4:455–479.
31. Lasic DD, Frederik PM, Stuart MC, Barenholz Y, Mcintosh TJ. Gelation of liposome interior. A novel method for drug encapsulation. FEBS Lett. 1992; 312(2–3):255–258. [PubMed: 1426260]
32. Lasic DD. Novel applications of liposomes. Trends Biotechnol. 1998; 16(7):307–321. [PubMed: 9675915]
33. Lasic, D.; Martin, F. Stealth Liposomes. CRC Press Inc; 1995.
34. Uchiyama K, Nagayasu A, Yamagiwa Y, Nishida T, Harashima H, Kiwada H. Effects of the size and fluidity of liposomes on their accumulation in tumors: A presumption of their interaction with tumors. International journal of pharmaceutics. 1995; 121:195–203.
35. Karathanasis E, Suryanarayanan S, Balusu SR, et al. Imaging nanoprobe for prediction of outcome of nanoparticle chemotherapy by using mammography. Radiology. 2009; 250(2):398–406. [PubMed: 19188313]
36. Karathanasis E, Chan L, Balusu SR, et al. Multifunctional nanocarriers for mammographic quantification of tumor dosing and prognosis of breast cancer therapy. Biomaterials. 2008; 29(36): 4815–4822. [PubMed: 18814908]
37. Karathanasis E, Park J, Agarwal A, et al. MRI mediated, non-invasive tracking of intratumoral distribution of nanocarriers in rat glioma. Nanotechnology. 2008; 19:9, 315101.
38. Toy R, Hayden E, Camann A, et al. Multimodal in vivo imaging exposes the voyage of nanoparticles in tumor microcirculation. ACS Nano. 2013; 7(4):3118–3129. [PubMed: 23464827]
39. Fukumura D, Jain RK. Tumor microenvironment abnormalities: causes, consequences, and strategies to normalize. J Cell Biochem. 2007; 101(4):937–949. [PubMed: 17171643]
40. Hobbs SK, Monsky WL, Yuan F, et al. Regulation of transport pathways in tumor vessels: role of tumor type and microenvironment. Proc Natl Acad Sci U S A. 1998; 95(8):4607–4612. [PubMed: 9539785]
41. Yuan F, Chen Y, Dellian M, Safabakhsh N, Ferrara N, Jain RK. Time-dependent vascular regression and permeability changes in established human tumor xenografts induced by an anti-vascular endothelial growth factor/vascular permeability factor antibody. Proc Natl Acad Sci U S A. 1996; 93(25):14765–14770. [PubMed: 8962129]
42. Karathanasis E, Chan L, Karumbaiah L, et al. Tumor vascular permeability to a nanoprobe correlates to tumor-specific expression levels of angiogenic markers. PLoS ONE. 2009; 4(6):e5843. [PubMed: 19513111]
43. Brix G, Bahner ML, Hoffmann U, Horvath A, Schreiber W. Regional blood flow, capillary permeability, and compartmental volumes: measurement with dynamic CT--initial experience. Radiology. 1999; 210(1):269–276. [PubMed: 9885619]
44. Wu H, Exner AA, Krupka TM, Weinberg BD, Patel R, Haaga JR. Radiofrequency ablation: post-ablation assessment using CT perfusion with pharmacological modulation in a rat subcutaneous tumor model. Acad Radiol. 2009; 16(3):321–331. [PubMed: 19201361]
45. Netti PA, Roberge S, Boucher Y, Baxter LT, Jain RK. Effect of transvascular fluid exchange on pressure-flow relationship in tumors: a proposed mechanism for tumor blood flow heterogeneity. Microvasc Res. 1996; 52(1):27–46. [PubMed: 8812751]
46. Nagamitsu A, Greish K, Maeda H. Elevating Blood Pressure as a Strategy to Increase Tumor-targeted Delivery of Macromolecular Drug SMANCS: Cases of Advanced Solid Tumors. Jpn J Clin Oncol. 2009
47. Kong G, Braun RD, Dewhirst MW. Hyperthermia enables tumor-specific nanoparticle delivery: effect of particle size. Cancer Res. 2000; 60(16):4440–4445. [PubMed: 10969790]
48. Gavze E, Shapiro M. Motion of inertial spheroidal particles in a shear flow near a solid wall with special application to aerosol transport in microgravity. Journal of Fluid Mechanics. 1998; 371:59–79.

49. Gentile F, Chiappini C, Fine D, et al. The effect of shape on the margination dynamics of non-neutrally buoyant particles in two-dimensional shear flows. J Biomech. 2008; 41(10):2312–2318. [PubMed: 18571181]
50. Chithrani BD, Ghazani AA, Chan WC. Determining the size and shape dependence of gold nanoparticle uptake into mammalian cells. Nano Lett. 2006; 6(4):662–668. [PubMed: 16608261]
51. Sharma G, Valenta DT, Altman Y, et al. Polymer particle shape independently influences binding and internalization by macrophages. J Control Release. 147(3):408–412. [PubMed: 20691741]
52. Geng Y, Dalhaimer P, Cai S, et al. Shape effects of filaments versus spherical particles in flow and drug delivery. Nat Nanotechnol. 2007; 2(4):249–255. [PubMed: 18654271]
53. Champion JA, Mitragotri S. Role of target geometry in phagocytosis. Proc Natl Acad Sci U S A. 2006; 103(13):4930–4934. [PubMed: 16549762]
54. Decuzzi P, Ferrari M. The adhesive strength of non-spherical particles mediated by specific interactions. Biomaterials. 2006; 27(30):5307–5314. [PubMed: 16797691]
55**. Peiris PM, Toy R, Doolittle E, et al. Imaging metastasis using an integrin-targeting chain-shaped nanoparticle. ACS Nano. 2012; 6(10):8783–8795. Evaluated the margination behavior and biodistribution of an oblate shaped integrin-targeting iron oxide nano-chain. [PubMed: 23005348]
56. Von Hoff DD, Layard MW, Basa P, et al. Risk factors for doxorubicin-induced congestive heart failure. Ann Intern Med. 1979; 91(5):710–717. [PubMed: 496103]
57. Schroeder A, Heller DA, Winslow MM, et al. Treating metastatic cancer with nanotechnology. Nat Rev Cancer. 2012; 12(1):39–50. [PubMed: 22193407]
58. Adiseshaiah PP, Hall JB, Mcneil SE. Nanomaterial standards for efficacy and toxicity assessment. Wiley Interdiscip Rev Nanomed Nanobiotechnol. 2010; 2(1):99–112. [PubMed: 20049834]
59. Cancer facts and figures 2011. American Cancer Society; 2011.
60. Tan SJ, Campolongo MJ, Luo D, Cheng W. Building plasmonic nanostructures with DNA. Nat Nano. 2011; 6(5):268–276.
61. Porel S, Singh S, Radhakrishnan TP. Polygonal gold nanoplates in a polymer matrix. Chem Commun (Camb). 2005; (18):2387–2389. [PubMed: 15877137]
62. Liu B, Xie J, Lee JY, Ting YP, Chen JP. Optimization of high-yield biological synthesis of single-crystalline gold nanoplates. J Phys Chem B. 2005; 109(32):15256–15263. [PubMed: 16852932]
63. Jin R, Cao Y, Mirkin CA, Kelly KL, Schatz GC, Zheng JG. Photoinduced conversion of silver nanospheres to nanoprisms. Science. 2001; 294(5548):1901–1903. [PubMed: 11729310]
64. Das SK, Das AR, Guha AK. Microbial synthesis of multishaped gold nanostructures. Small. 2010; 6(9):1012–1021. [PubMed: 20376859]
65. Ah CS, Yun YJ, Park HJ, Kim WJ, Ha DH, Yun WS. Size-controlled synthesis of machinable single crystalline gold nanoplates. Chem Mat. 2005; 17(22):5558–5561.
66. Tao AR, Ceperley DP, Sinsermsuksakul P, Neureuther AR, Yang P. Self-organized silver nanoparticles for three-dimensional plasmonic crystals. Nano Lett. 2008; 8(11):4033–4038. [PubMed: 18928325]
67. Wyrwa D, Beyer N, Schmid G. One-dimensional arrangements of metal nanoclusters. Nano Letters. 2002; 2(4):419–421.
68. Sun YG, Mayers BT, Xia YN. Template-engaged replacement reaction: A one-step approach to the large-scale synthesis of metal nanostructures with hollow interiors. Nano Letters. 2002; 2(5):481–485.
69. Kim DY, Im SH, Park OO, Lim YT. Evolution of gold nanoparticles through Catalan, Archimedean, and Platonic solids. Crystengcomm. 2010; 12(1):116–121.
70. Kim F, Connor S, Song H, Kuykendall T, Yang PD. Platonic gold nanocrystals. Angew Chem-Int Edit. 2004; 43(28):3673–3677.
71. Tao A, Sinsermsuksakul P, Yang P. Tunable plasmonic lattices of silver nanocrystals. Nat Nanotechnol. 2007; 2(7):435–440. [PubMed: 18654329]
72. Seo D, Il Yoo C, Chung IS, Park SM, Ryu S, Song H. Shape adjustment between multiply twinned and single-crystalline polyhedral gold nanocrystals: Decahedra, icosahedra, and truncated tetrahedra. J Phys Chem C. 2008; 112(7):2469–2475.

73. Murphy CJ, Gole AM, Hunyadi SE, Orendorff CJ. One-dimensional colloidal gold and silver nanostructures. Inorg Chem. 2006; 45:7544–7554. [PubMed: 16961339]
74. Huo Z, Tsung CK, Huang W, Zhang X, Yang P. Sub-two nanometer single crystal au nanowires. Nano Lett. 2008; 8:2041–2044. [PubMed: 18537294]
75. Zhao N. Controlled synthesis of gold nanobelts and nanocombs in aqueous mixed surfactant solutions. Langmuir. 2008; 24:991–998. [PubMed: 18173292]
76. Wiley BJ. Synthesis and electrical characterization of silver nanobeams. Nano Lett. 2006; 6:2273–2278. [PubMed: 17034096]
77. Xiong Y. Synthesis and mechanistic study of palladium nanobars and nanorods. J AM CHEM SOC. 2007; 129:3665–3675. [PubMed: 17335211]
78. Ni W, Yang Z, Chen H, Li L, Wang J. Coupling between molecular and plasmonic resonances in freestanding dye-gold nanorod hybrid nanostructures. J AM CHEM SOC. 2008; 130:6692–6693. [PubMed: 18457390]
79. Wijaya A, Schaffer SB, Pallares IG, Hamad-Schifferli K. Selective release of multiple DNA oligonucleotides from gold nanorods. ACS Nano. 2008; 3:80–86. [PubMed: 19206252]
80. Mulvihill MJ, Ling XY, Henzie J, Yang P. Anisotropic etching of silver nanoparticles for plasmonic structures capable of single-particle SERS. J AM CHEM SOC. 2009; 132:268–274. [PubMed: 20000421]
81. Liao HG, Jiang YX, Zhou ZY, Chen SP, Sun SG. Shape-controlled synthesis of gold nanoparticles in deep eutectic solvents for studies of structure-functionality relationships in electrocatalysis. Angew Chem Int Ed. 2008; 47:9100–9103.
82. Cheng WL, Dong SJ, Wang EK. Synthesis and self-assembly of cetyltrimethylammonium bromide-capped gold nanoparticles. Langmuir. 2003; 19:9434–9439.
83. Chen S, Wang ZL, Ballato J, Foulger SH, Carroll DL. Monopod, bipod, tripod, and tetrapod gold nanocrystals. J Am Chem Soc. 2003; 125(52):16186–16187. [PubMed: 14692749]
84. Perro A, Reculusa S, Pereira F, et al. Towards large amounts of Janus nanoparticles through a protection-deprotection route. Chem Commun (Camb). 2005; (44):5542–5543. [PubMed: 16358056]
85. Decuzzi P, Godin B, Tanaka T, et al. Size and shape effects in the biodistribution of intravascularly injected particles. J Control Release. 2009; 141(3):320–327. [PubMed: 19874859]
86. Rolland JP, Maynor BW, Euliss LE, Exner AE, Denison GM, Desimone JM. Direct fabrication and harvesting of monodisperse, shape-specific nanobiomaterials. J Am Chem Soc. 2005; 127(28): 10096–10100. [PubMed: 16011375]
87. Xu Y, Zheng L, Xie Y. From synthetic montroseite VOOH to topochemical paramontroseite VO2 and their applications in aqueous lithium ion batteries. Dalton Trans. 2010; 39(44):10729–10738. [PubMed: 20941433]
88. Muro S, Garnacho C, Champion JA, et al. Control of endothelial targeting and intracellular delivery of therapeutic enzymes by modulating the size and shape of ICAM-1-targeted carriers. Mol Ther. 2008; 16(8):1450–1458. [PubMed: 18560419]
89. Doshi N, Zahr AS, Bhaskar S, Lahann J, Mitragotri S. Red blood cell-mimicking synthetic biomaterial particles. Proc Natl Acad Sci U S A. 2009; 106(51):21495–21499. [PubMed: 20018694]
90. Cheng WL, Steinhart M, Gosele U, Wehrspohn R. Tree-like alumina nanopores generated in a non-steady-state anodization. J Mater Chem. 2007; 17:3493–3495.
91. Qin Y, Song Y, Sun NJ, Zhao N, Li MX, Qi LM. Ionic liquid-assisted growth of single-crystalline dendritic gold nanostructures with a three-fold symmetry. Chem Mat. 2008; 20(12):3965–3972.
92. Dai Q, Worden JG, Trullinger J, Huo Q. A “nanonecklace” synthesized from monofunctionalized gold nanoparticles. Journal of the American Chemical Society. 2005; 127(22):8008–8009. [PubMed: 15926813]
93. Peiris PM, Bauer L, Toy R, et al. Enhanced Delivery of Chemotherapy to Tumors Using a Multicomponent Nanochain with Radio-Frequency-Tunable Drug Release. ACS Nano. 2012; 6(5): 4157–4168. [PubMed: 22486623]
94. Sardar R, Shumaker-Parry JS. Asymmetrically functionalized gold nanoparticles organized in one-dimensional chains. Nano Lett. 2008; 8(2):731–736. [PubMed: 18269261]

95. Canelas DA, Herlihy KP, Desimone JM. Top-down particle fabrication: control of size and shape for diagnostic imaging and drug delivery. Wiley Interdiscip Rev Nanomed Nanobiotechnol. 2009; 1(4):391–404. [PubMed: 20049805]

96. Piner RD, Zhu J, Xu F, Hong S, Mirkin CA. “Dip-Pen” nanolithography. Science. 1999; 283(5402):661–663. [PubMed: 9924019]

97. Albanese A, Tang PS, Chan WC. The effect of nanoparticle size, shape, and surface chemistry on biological systems. Annual review of biomedical engineering. 2012; 14:1–16.

98. Petros RA, Desimone JM. Strategies in the design of nanoparticles for therapeutic applications. Nat Rev Drug Discov. 9(8):615–627. [PubMed: 20616808]

99. Duan X, Li Y. Physicochemical characteristics of nanoparticles affect circulation, biodistribution, cellular internalization, and trafficking. Small. 9(9–10):1521–1532. [PubMed: 23019091]

100. Shukla S, Wen AM, Ayat NR, et al. Biodistribution and clearance of a filamentous plant virus in healthy and tumor-bearing mice. Nanomedicine. 2013

101. Sardar R, Shumaker-Parry JS. Asymmetrically functionalized gold nanoparticles organized in one-dimensional chains. Nano Letters. 2008; 8(2):731–736. [PubMed: 18269261]

102. Owens DE 3rd, Peppas NA. Opsonization, biodistribution, and pharmacokinetics of polymeric nanoparticles. International journal of pharmaceutics. 2006; 307(1):93–102. [PubMed: 16303268]

103*. Champion JA, Katare YK, Mitragotri S. Particle shape: a new design parameter for micro- and nanoscale drug delivery carriers. J Control Release. 2007; 121(1–2):3–9. Studied the effect of contact angle on the phagocytosis of nanoparticles of different shapes. [PubMed: 17544538]

104. Vinogradov SV, Bronich TK, Kabanov AV. Nanosized cationic hydrogels for drug delivery: preparation, properties and interactions with cells. Adv Drug Deliv Rev. 2002; 54(1):135–147. [PubMed: 11755709]

105. Choi HS, Liu W, Misra P, et al. Renal clearance of quantum dots. Nat Biotechnol. 2007; 25(10): 1165–1170. [PubMed: 17891134]

106. Moghimi SM, Hedeman H, Christy NM, Illum L, Davis SS. Enhanced hepatic clearance of intravenously administered sterically stabilized microspheres in zymosan-stimulated rats. J Leukoc Biol. 1993; 54(6):513–517. [PubMed: 8245702]

107. Porter CJ, Moghimi SM, Illum L, Davis SS. The polyoxyethylene/polyoxypropylene block co-polymer poloxamer-407 selectively redirects intravenously injected microspheres to sinusoidal endothelial cells of rabbit bone marrow. FEBS Lett. 1992; 305(1):62–66. [PubMed: 1633861]

108. Li SD, Huang L. Pharmacokinetics and biodistribution of nanoparticles. Molecular pharmaceutics. 2008; 5(4):496–504. [PubMed: 18611037]

109. Tollis S, Dart AE, Tzircotis G, Endres RG. The zipper mechanism in phagocytosis: energetic requirements and variability in phagocytic cup shape. BMC Syst Biol. 4:149. [PubMed: 21059234]

110. Gabizon AD. Papahadjopoulos. Liposome formulations with prolonged circulation time in blood and enhanced uptake by tumors. Proc Natl Acad Sci. 1988; 85:6949–6953. [PubMed: 3413128]

111. Arnida, Janat-Amsbury MM, Ray A, Peterson CM, Ghandehari H. Geometry and surface characteristics of gold nanoparticles influence their biodistribution and uptake by macrophages. Eur J Pharm Biopharm. 77(3):417–423. [PubMed: 21093587]

112. Huang X, Li L, Liu T, et al. The shape effect of mesoporous silica nanoparticles on biodistribution, clearance, and biocompatibility in vivo. ACS Nano. 5(7):5390–5399. [PubMed: 21634407]

113. Shapiro, EGaM. Particles in a Shear Flow Near a Solid Wall: Effect of Nonsphericity on Forces and Velocities. Int J Multiphase Flow. 1996

114. Decuzzi P, Lee S, Bhushan B, Ferrari M. A theoretical model for the margination of particles within blood vessels. Ann Biomed Eng. 2005; 33(2):179–190. [PubMed: 15771271]

115. Gentile F, Curcio A, Indolfi C, Ferrari M, Decuzzi P. The margination propensity of spherical particles for vascular targeting in the microcirculation. J Nanobiotechnology. 2008; 6:9. [PubMed: 18702833]

116*. Toy R, Hayden E, Shoup C, Baskaran H, Karathanasis E. The effects of particle size, density and shape on margination of nanoparticles in microcirculation. Nanotechnology. 22(11):115101.

Studied the effect of nanoparticle size, nanoparticle shape, and blood flow rate on nanoparticle margination. [PubMed: 21387846]

117. Park J, Butler JE. Analysis of the Migration of Rigid Polymers and Nanorods in a Rotating Viscometric Flow. Macromolecules. 2010; (43):2535–2543.

118**. Adriani G, De Tullio MD, Ferrari M, et al. The preferential targeting of the diseased microvasculature by disk-like particles. Biomaterials. 33(22):5504–5513. Evaluated the margination behavior of spheres, discs, and rods at different rates and calculated the hydrodynamic forces acting on these particles. [PubMed: 22579236]

119. Thompson AJ, Mastria EM, Eniola-Adefeso O. The margination propensity of ellipsoidal micro/nanoparticles to the endothelium in human blood flow. Biomaterials. 34(23):5863–5871. [PubMed: 23642534]

120. Doshi N, Prabhakarpandian B, Rea-Ramsey A, Pant K, Sundaram S, Mitragotri S. Flow and adhesion of drug carriers in blood vessels depend on their shape: a study using model synthetic microvascular networks. J Control Release. 146(2):196–200. [PubMed: 20385181]

121. Charoenphol P, Onyskiw PJ, Carrasco-Teja M, Eniola-Adefeso O. Particle-cell dynamics in human blood flow: implications for vascular-targeted drug delivery. J Biomech. 45(16):2822–2828. [PubMed: 23010218]

122. Jain A, Munn LL. Determinants of leukocyte margination in rectangular microchannels. PLoS One. 2009; 4(9):e7104. [PubMed: 19768109]

123. Hong S, Leroueil PR, Majoros IJ, Orr BG, Baker JR Jr, Banaszak Holl MM. The binding avidity of a nanoparticle-based multivalent targeted drug delivery platform. Chem Biol. 2007; 14(1):107–115. [PubMed: 17254956]

124. Muro S, Dziubla T, Qiu W, et al. Endothelial targeting of high-affinity multivalent polymer nanocarriers directed to intercellular adhesion molecule 1. J Pharmacol Exp Ther. 2006; 317(3):1161–1169. [PubMed: 16505161]

125. Calderon AJ, Bhowmick T, Leferovich J, et al. Optimizing endothelial targeting by modulating the antibody density and particle concentration of anti-ICAM coated carriers. J Control Release. 150(1):37–44. [PubMed: 21047540]

126. Saul JM, Annapragada A, Natarajan JV, Bellamkonda RV. Controlled targeting of liposomal doxorubicin via the folate receptor in vitro. J Control Release. 2003; 92(1–2):49–67. [PubMed: 14499185]

127. Rangger C, Helbok A, Von Guggenberg E, et al. Influence of PEGylation and RGD loading on the targeting properties of radiolabeled liposomal nanoparticles. Int J Nanomedicine. 7:5889–5900. [PubMed: 23226020]

128. Decuzzi P, Ferrari M. The receptor-mediated endocytosis of nonspherical particles. Biophys J. 2008; 94(10):3790–3797. [PubMed: 18234813]

129. Ghaghada KB, Saul J, Natarajan JV, Bellamkonda RV, Annapragada AV. Folate targeting of drug carriers: a mathematical model. J Control Release. 2005; 104(1):113–128. [PubMed: 15866339]

130. Jeppesen C, Wong JY, Kuhl TL, et al. Impact of polymer tether length on multiple ligand-receptor bond formation. Science. 2001; 293(5529):465–468. [PubMed: 11463908]

131. Hak S, Helgesen E, Hektoen HH, et al. The effect of nanoparticle polyethylene glycol surface density on ligand-directed tumor targeting studied in vivo by dual modality imaging. ACS Nano. 6(6):5648–5658. [PubMed: 22671719]

132. Mcneeley KM, Karathanasis E, Annapragada AV, Bellamkonda RV. Masking and triggered unmasking of targeting ligands on nanocarriers to improve drug delivery to brain tumors. Biomaterials. 2009; 30(23–24):3986–3995. [PubMed: 19427688]

133*. Kolhar P, Anselmo AC, Gupta V, et al. Using shape effects to target antibody-coated nanoparticles to lung and brain endothelium. Proc Natl Acad Sci U S A. Compared the binding and attachment of antibody-coated nano-rods and nano-spheres.

134. Varma R, Mayor S. GPI-anchored proteins are organized in submicron domains at the cell surface. Nature. 1998; 394(6695):798–801. [PubMed: 9723621]

135. Sabharanjak S, Sharma P, Parton RG, Mayor S. GPI-anchored proteins are delivered to recycling endosomes via a distinct cdc42-regulated, clathrin-independent pinocytic pathway. Dev Cell. 2002; 2(4):411–423. [PubMed: 11970892]

136. Rodal SK, Skretting G, Garred O, Vilhardt F, Van Deurs B, Sandvig K. Extraction of cholesterol with methyl-beta-cyclodextrin perturbs formation of clathrin-coated endocytic vesicles. Mol Biol Cell. 1999; 10(4):961–974. [PubMed: 10198050]

137. Nesterov A, Wiley HS, Gill GN. Ligand-induced endocytosis of epidermal growth factor receptors that are defective in binding adaptor proteins. Proc Natl Acad Sci U S A. 1995; 92(19): 8719–8723. [PubMed: 7568004]

138. Edidin M. Lipid microdomains in cell surface membranes. Curr Opin Struct Biol. 1997; 7(4):528–532. [PubMed: 9266174]

139. Griffiths G, Back R, Marsh M. A quantitative analysis of the endocytic pathway in baby hamster kidney cells. J Cell Biol. 1989; 109(6 Pt 1):2703–2720. [PubMed: 2592402]

140. Hansen SH, Sandvig K, Van Deurs B. Internalization efficiency of the transferrin receptor. Exp Cell Res. 1992; 199(1):19–28. [PubMed: 1735458]

141. Kamen BA, Capdevila A. Receptor-mediated folate accumulation is regulated by the cellular folate content. Proc Natl Acad Sci U S A. 1986; 83(16):5983–5987. [PubMed: 3461471]

142. Hlavacek WS, Posner RG, Perelson AS. Steric effects on multivalent ligand-receptor binding: exclusion of ligand sites by bound cell surface receptors. Biophys J. 1999; 76(6):3031–3043. [PubMed: 10354429]

143. Ghaghada KB, Saul J, Natarajan JV, Bellamkonda RV, Annapragada AV. Folate targeting of drug carriers: A mathematical model. J Control Release. 2005; 104(1):113–128. [PubMed: 15866339]

144. Yang K, Ma YQ. Computer simulation of the translocation of nanoparticles with different shapes across a lipid bilayer. Nat Nanotechnol. 5(8):579–583. [PubMed: 20657599]

145. Smith BR, Kempen P, Bouley D, et al. Shape matters: intravital microscopy reveals surprising geometrical dependence for nanoparticles in tumor models of extravasation. Nano Lett. 12(7): 3369–3377. [PubMed: 22650417]

146. Barua S, Yoo JW, Kolhar P, Wakankar A, Gokarn YR, Mitragotri S. Particle shape enhances specificity of antibody-displaying nanoparticles. Proc Natl Acad Sci U S A. 2013; 110(9):3270–3275. [PubMed: 23401509]

147. Peiris PM, Tam M, Vicente P, et al. On-Command Drug Release from Nanochains Inhibits Growth of Breast Tumors. Pharm Res.

148. Jain PK, Lee KS, El-Sayed IH, El-Sayed MA. Calculated absorption and scattering properties of gold nanoparticles of different size, shape, and composition: applications in biological imaging and biomedicine. J Phys Chem B. 2006; 110(14):7238–7248. [PubMed: 16599493]

Executive Summary

Introduction

- A nanoparticle's shape and size dictates its rate of margination and its ability to bind to cell membranes.
- A plethora of fabrication methods enables the manufacturing of nanoparticles of a wide variety of shapes and sizes.

The effect of nanoparticle shape on biodistribution and macrophage uptake

- The rate of internalization of a non-spherical nanoparticle depends on its angular orientation relative to the cell membrane.
- Hydrodynamic forces impact the rate of macrophage uptake of a nanoparticle.

Modifying nanoparticle shape to enhance margination

- Hydrodynamic forces impact the margination of nanoparticles. Non-spherical particles have a higher tendency to marginate and escape the blood flow.
- Shear rate, vessel geometry, hematocrit, and blood flow pattern influence the margination of nanoparticles of different shapes to different degrees.

Tailoring nanoparticle shape to maximize binding affinity

- Modifying a nanoparticle's shape leads to changes in ligand presentation, which ultimately affects nanoparticle binding avidity.

Effect of nanoparticle shape on tumor deposition and therapeutic efficacy

Tailoring the shape of a nanoparticle can enhance deposition into a tumor through both passive and active mechanisms, which leads to improved therapeutic efficacy.

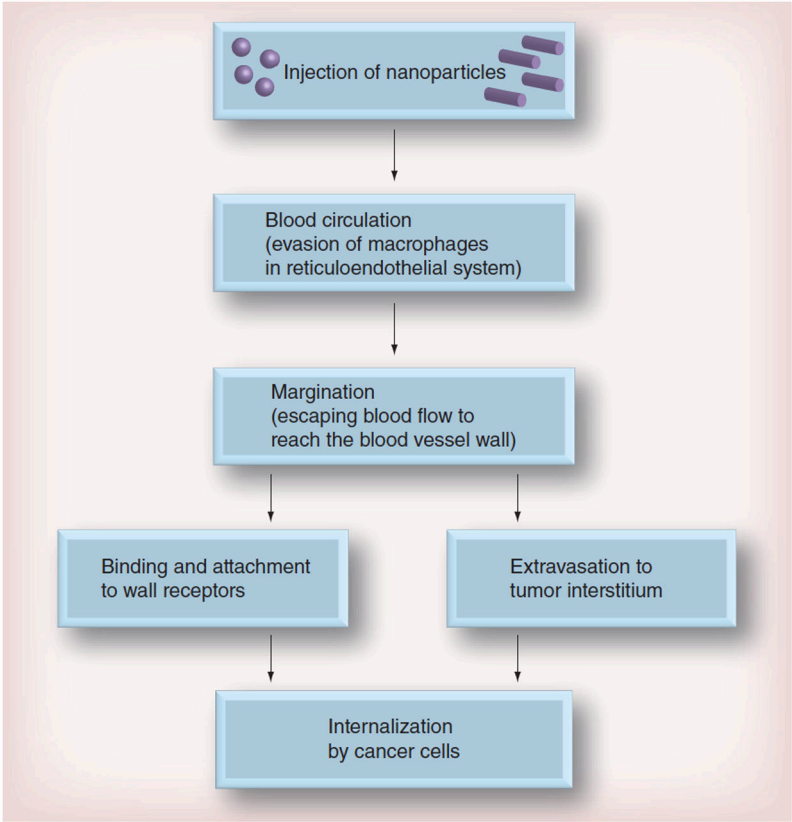

Figure 1. Schematic of biological processes which influence nanoparticle delivery

A nanoparticle must be able to circulate, marginate, and bind to a vascular target or extravasate into the tumor interstitium before it can be internalized by a cancer cell.

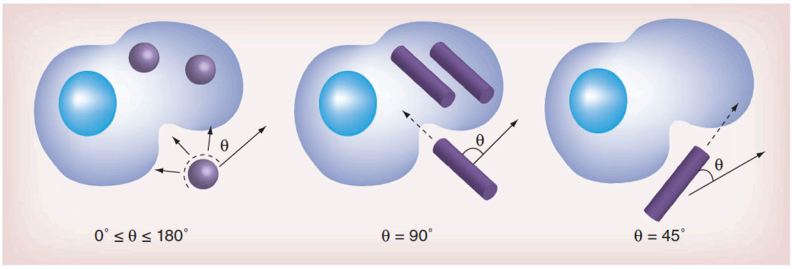

Figure 2. Effect of contact angle (θ) on the rate of nanoparticle internalization

Rod-shaped nanoparticles internalize most quickly when their major axis is perpendicular to the cell membrane. As the rod is oriented more tangentially to the cell membrane, the rate of internalization decreases. This is due to the increased difficulty to "wrap" the nanoparticle. Because spherical nanoparticles are symmetric, they internalize at a rate independent of θ.

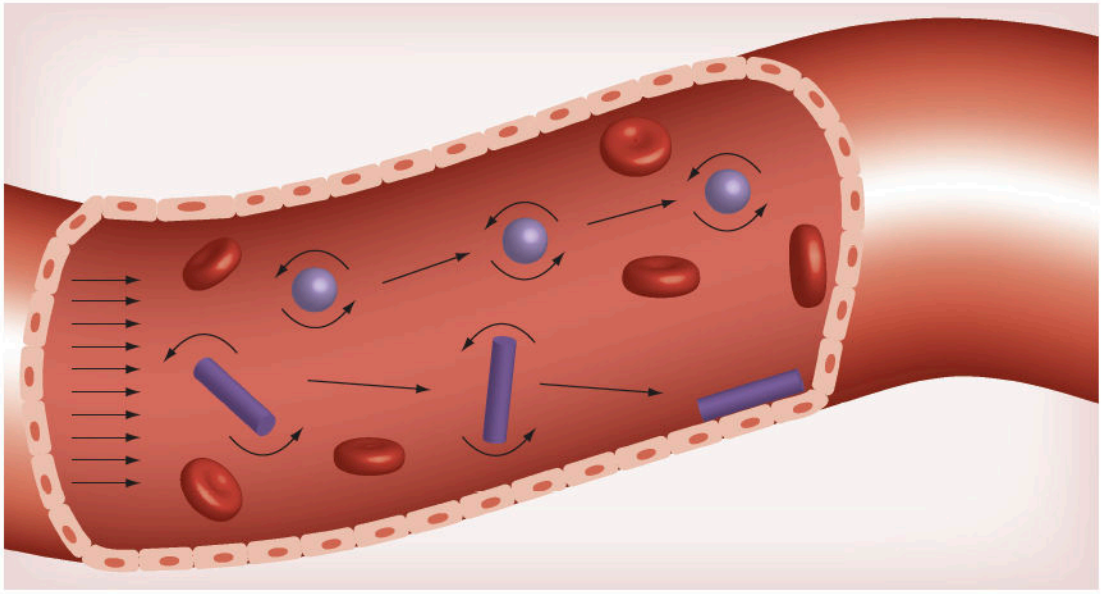

Figure 3. Effect of shape on nanoparticle margination

Spherical nanoparticles tend to remain in the center of the flow. Variable forces and torques exerted on rods under flow allow them to marginate and drift towards the vessel wall, where they are able to bind to wall receptors or extravasate through gaps between cells of the endothelium.

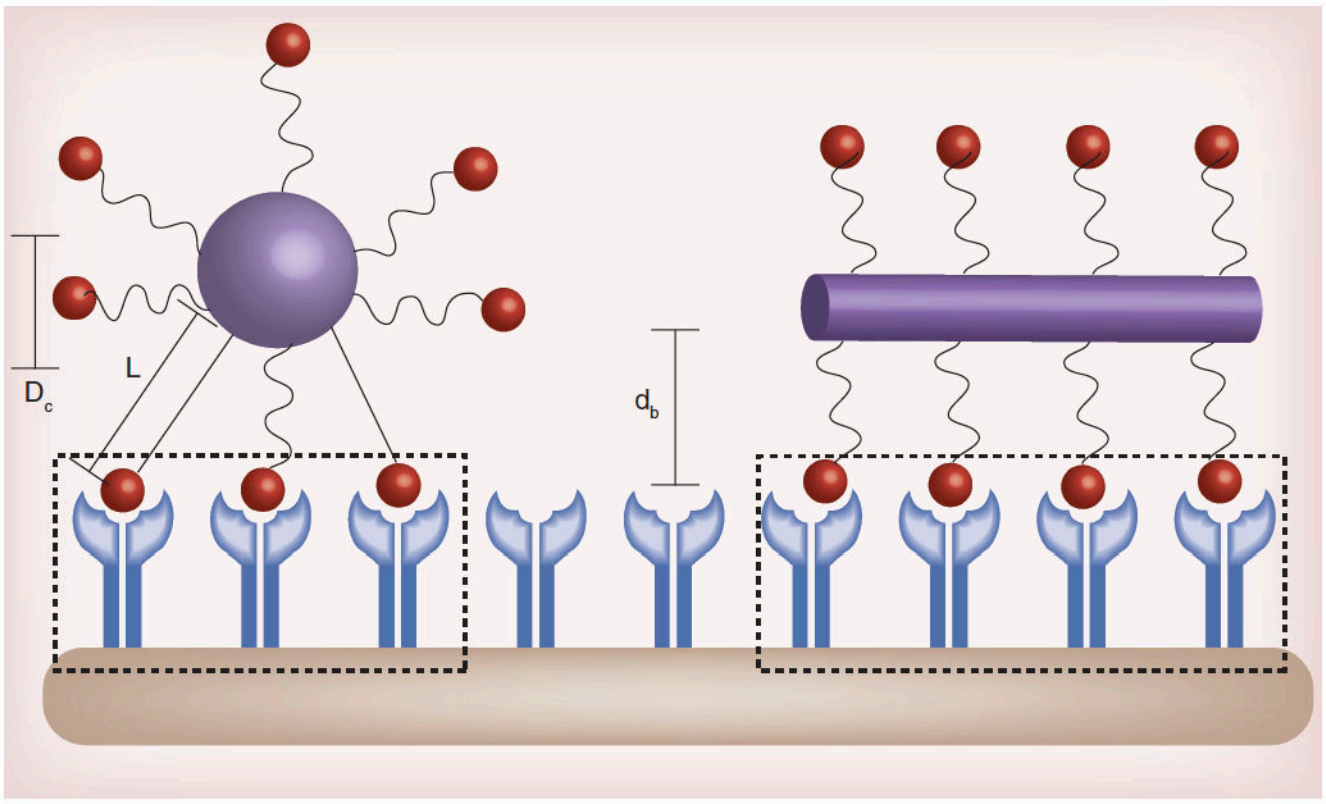

Figure 4. Effect of shape on nanoparticle binding avidity

Shape, ligand length, and polymer flexibility all play a role in the active fractional area of a nano-carrier (AFAC). For a sphere, the AFAC is defined as $(L\text{-}d_B)/D_c$, where L is the length of the ligand, d_b is the binding distance between the nanoparticle and the receptor, and D_c is the diameter of the nano-carrier. For particles with equal surface area, the ligand length, binding distance, and shape affects AFAC.

Table 1

Non spherical nanoparticles of various shapes fabricated in recent years.

Shape	Types	Materials	Methods	Ref.
2-D polygonal	Triangle, Square, Pentagon, Hexagon, Disc, Nanoring	Au, Ag, Pt, Pd, Triacrylate resin, PLA[$], PEG[#]-diacrylate, poly(pyrrole)	PRINT®[*] lithography, microfluidics, photopolymerization	[60–67]
3-D Polyhedral	Tetrahedron, Cube, Decahedron, Octahedron, Icosahedrons, Hollow nanocage	Au, Ag, Pt, Pd, PLA, poly(pyrrole), PEG-(diacrylate),	PRINT®, Step flash imprint lithography, Microfluidics	[68–72, 100]
Rod-like	Nanobar, Nanorod, Nanobone, Nanobeam, Nanobelt, Nanowires	Au, Ag, Pt, Fe, Cu, Cr, Co metals, alloys, and oxides	Stretching spherical particle, Electrochemical deposition, self assembly, Solution-phase chemical reduction	[73–79]
Branched	Monopod, Bipod, Tripod, Tetrapod, Star-shaped, Octapod	Au, CdS, CdSe, CdTe, MnS, and ZnO	Thermal and chemical vapor deposition, Solution-phase chemical reduction	[80–82]
Complex	Snowflakes, Flowers, Thorns, hemispheres, Cones, Urchins, Filamentous particles, Biconcave discoids, Worms, Trees, Dendrites, Necklaces, Chains	Au, Ag, Pt, Fe, Cu, Ru, Co, metals, alloys, and oxides, Si and Si oxides	Hydrothermal, PRINT®, Solid phase synthesis, self assembly, wet chemical synthesis, Solution-phase chemical reduction,	[8, 9, 52, 55, 81, 84–93, 101]

[$] PLA- Poly lactic acid

[#] PEG- Poly(ethylene glycol),

[*] PRINT® - Particle Replication In Non-wetting Templates